Magnetic Kondo regimes in a frustrated half-filled trimer

Krzysztof P. Wójcik [1,2,*] Ireneusz Weymann [3] and Johann Kroha [2]
[1]*Institute of Molecular Physics, Polish Academy of Sciences, Smoluchowskiego 17, 60-179 Poznań, Poland*
[2]*Physikalisches Institut, Universität Bonn, Nussallee 12, D-53115 Bonn, Germany*
[3]*Faculty of Physics, A. Mickiewicz University, Uniwersytetu Poznańskiego 2, 61-614 Poznań, Poland*

(Received 24 March 2020; revised 2 July 2020; accepted 6 July 2020; published 24 July 2020)

We analyze theoretically the phase diagram of a triangular triple quantum dot with strong on-site repulsion coupled to ferromagnetic leads. This model includes the competition of magnetic ordering of local or itinerant magnetic moments, geometric frustration, and Kondo screening. We identify all the phases resulting from this competition. We find that three Kondo phases—the conventional one, the two-stage underscreened one, and the one resulting from the ferromagnetic Kondo effect—can be realized at zero temperature, and all are very susceptible to the proximity of ferromagnetic leads. In particular, we find that the quantum dots are spin polarized in each of these phases. Further, we discuss the fate of the phases at nonzero temperatures, where a plethora of competing energy scales gives rise to a complex landscape of crossovers. Each Kondo regime splits into a pair of phases, one not magnetized and one comprising magnetically polarized quantum dots. We discuss our results in the context of heavy-fermion physics in frustrated Kondo lattices.

DOI: 10.1103/PhysRevB.102.045144

I. INTRODUCTION

Heavy-fermion systems are magnetic materials where rare-earth magnetic ions reside on a lattice, and their $4f$ electrons carrying local moments hybridize with the itinerant electrons of a conduction band [1]. The resulting spin-exchange coupling between local and itinerant moments leads to a Kondo effect and, hence, a heavy band near the Fermi level [1,2]. The competition between local spin exchange and nonlocal spin coupling mediated by the Ruderman-Kittel-Kasuya-Yosida (RKKY) interaction [3–5] can induce a quantum phase transition (QPT) from a paramagnetic Kondo-screened phase with expanded Fermi volume to a magnetically ordered phase [1]. However, experiments indicate that in some heavy-fermion systems the ordered and the Kondo phases may be separated by a state which is neither long-range ordered nor completely Kondo screened [6–8]. This suggests that in the global heavy-fermion phase diagram, magnetic frustration may play an additional, important role [9–13]. The latter may be induced by the long-range, oscillatory nature of the RKKY interaction. Frustration in insulating spin lattices has been largely treated on the basis of the two-dimensional Shastry-Sutherland model [14,15]. However, the presence of a conduction band with potential Kondo singlet formation introduces another complication. Despite analytical [11,16] and numerical [17,18] treatments of frustrated Kondo lattice models, a complete understanding of all the phases possible by multiple tuning parameters is still lacking. The problem becomes even more complex in systems where the local magnetic moments sit on several crystallographically inequivalent lattice sites [19–24] or where magnetic order may even coexist with a Kondo-screened phase [25].

In the present paper, to shed more light on the intriguing interplay of the aforementioned effects, we take a minimal quantum impurity model, where frustration, Kondo screening, and magnetic correlations coexist and compete with each other. In particular, we consider a quantum-dot (QD) trimer coupled to a single spin-polarized screening channel in the geometry depicted in Fig. 1(a). The three QDs, exhibiting strong on-site Coulomb interactions, are assumed to form a triangular constellation. The first QD (QD1) is embedded between two leads made of a ferromagnetic metal. This dot is coupled to the second (QD2) and third (QD3) QDs, respectively, via the hopping matrix element t, while QD2 and QD3 are coupled by the frustrating hopping t'. This model incorporates the essential features of the interplay of local Kondo screening, magnetic ordering (magnetic dimer formation), and geometric frustration, parameterized by the ratio t'/t. It also takes into account the inequivalence of Kondo sites in that only the first dot is coupled to the leads. This is a simplified, numerically tractable description of a situation where a spatially varying density of states or exchange coupling may lead to an exponential suppression of the Kondo temperature on some of the Kondo sites, i.e., an effective decoupling of some screening channels [26–28]. A possible coexistence of itinerant magnetic ordering and Kondo screening can be analyzed by allowing for a magnetic polarization of the leads. Such a quantum impurity model has such advantage that, despite its complex physics, it can be reliably analyzed by the numerical renormalization group (NRG) method [29], and can be realized in QD experiments where all system parameters can be continuously tuned, which is usually difficult in lattice systems. Note also that a quantum impurity model of this type would emerge in a cluster dynamical mean-field theory [30,31] of geometrically frustrated Kondo or Anderson lattice systems.

Nonmagnetic Kondo trimers have been extensively examined theoretically [32–47], also in the case of few-channel screening [48–52]. The presence of a QPT separating the

*kpwojcik@ifmpan.poznan.pl

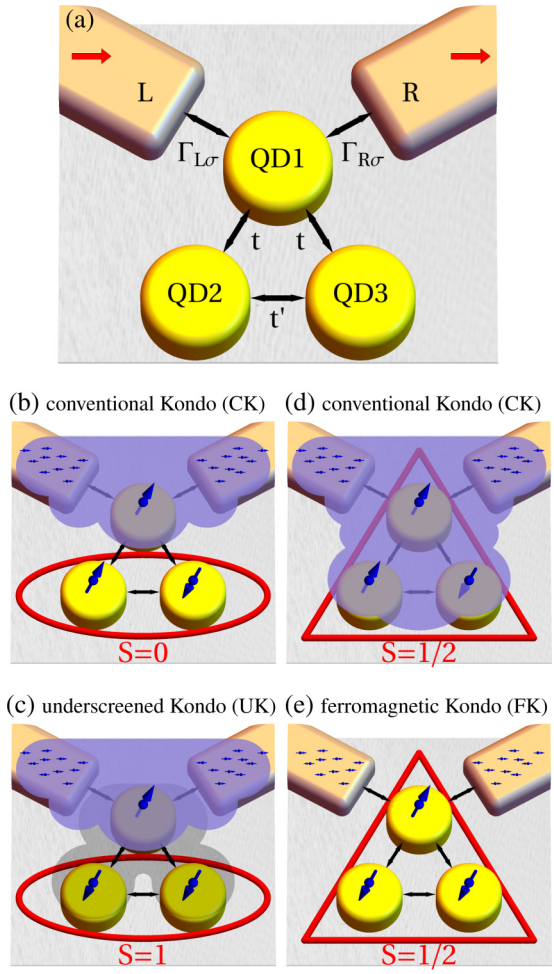

FIG. 1. (a) Schematic of the considered Kondo trimer, consisting of three *quantum dots*, denoted as QD1, QD2, QD3, coupled to ferromagnetic left (L) and right (R) leads with spin-dependent coupling strengths $\Gamma_{L(R)\sigma}$. (b)–(e) Illustrative presentation of possible orientations of the quantum dot spins (illustrated as arrows) and phases that may arise in the system: (b) the *conventional Kondo* (CK) phase with weak interdot hopping t, (c) the *underscreened Kondo* (UK) phase, (d) the CK phase for stronger t, and (e) the *ferromagnetic Kondo* (FK) phase. S denotes the spin of the indicated fragment of the trimer system. The semi-transparent shapes represent schematically the Kondo screening clouds. See Sec. II for more details.

conventional Kondo (CK) phase [53,54] from the exotic *ferromagnetic Kondo* (FK) regime hosting a nonscreened local magnetic moment and singular dynamics at low temperatures [55,56] is well established [38]. A separation of the *underscreened Kondo* (UK) phase [56,57] from the FK one by zero-temperature crossover has been also analyzed [39]. In addition, QD trimers have also been widely studied in the context of quantum computing [58–66] and spintronics [67–72]. However, especially the latter remains quite detached from the studies of strongly correlated Kondo physics. In particular, a comprehensive analysis of all phases in the presence of magnetic order seems to be missing. One of the aims of this paper is therefore to fill this gap. We show that due to the ferromagnetic proximity effect, all Kondo phases (namely CK, FK, and UK) turn into their spin-polarized counterparts (which we denote by CK′, FK′ and UK′, correspondingly) for arbitrarily small frustrating coupling t'.

While in the existing literature, the trimer phase diagrams have been investigated mainly at vanishing temperature, we show that the $T \to 0$ limit is irrelevant for experiments in certain parameter regimes. Moreover, even though often the quantum impurity systems can generally be understood in terms of a few stable $T \to 0$ phases and the QPTs between them [28,32,73–78], a number of cases, where continuous crossovers significantly alter the physics, are also known [79–82], especially in the context of competition between the Kondo effect and the spin polarization caused by ferromagnetic leads [83–85].

We demonstrate that in the presence of frustration, the Kondo phases are spin polarized in the $T \to 0$ limit and remain so up to experimentally relevant temperatures even for very weak frustrating coupling. This means that our results are actually relevant also for nearly linear trimers with t' interpreted as a weak next-nearest-neighbor hopping; cf. Fig. 1(a). Additionally, a finite-temperature crossover links the corresponding spin-polarized and spin-isotropic phases. As can be expected [86], the UK' phase is especially fragile to the presence of magnetic leads, which tangibly differs it from the FK' phase, where the spin polarization of relevant quantum dots is significantly smaller. This is in contrast to the huge resemblance between the nonmagnetic UK and FK regimes [39].

It is also important to note that a number of experiments on triple quantum dot systems have been performed in the context of quantum computing [87–95] or charge frustrations [65], and to study the triple QD's Kondo physics [35]. We therefore believe that our results will foster further experimental efforts to examine different competing phenomena in correlated magnetic nanostructures, especially in coupled QD systems.

As the study concerns quite a rich model, to increase its accessibility we describe the results beginning with the most general features and provide more precise understanding in subsequent sections. We start by presenting a qualitative physical picture of the system in Sec. II, setting the stage for the landscape of phases emerging in the presence of spin-polarized leads. Then, having presented the details of the model and methodology in Sec. III, we list and estimate all the relevant energy scales in Sec. IV. The general structure of the phase diagram in the space of interdot hopping t, frustrating hopping t', and temperature is outlined in Sec. V. Finally, the numerical results allowing us to precisely pinpoint the borders between the phases are presented in Sec. VI, corroborating estimations done in Sec. IV. The paper is concluded in Sec. VII.

II. QUALITATIVE PHYSICAL PICTURE

The system depicted in Fig. 1(a) comprises several couplings, each of them driving some kind of spin ordering even in the absence of lead magnetization. In the present section, we therefore briefly summarize all known Kondo phases of such system [38,39], in a form suitable for the comparison with our results presented in further sections.

First, the possibility of electron hopping between the first and other dots, described by hopping amplitude t, tends to align the spin of the first dot antiparallelly with respect to the spins of the other dots (QD2 and QD3). On the other hand, the direct hopping between QD2 and QD3, t', frustrates this order by trying to bind the electrons residing the second and third dot into a spin singlet. This becomes possible when the QD1 spin gets screened by the leads via the (conventional) Kondo effect. Such scenario is presented schematically in Fig. 1(b).

The situation is completely different in the case of relatively small t'. Then the QD2-QD3 direct exchange interaction is weak and can be overcome by the superexchange mediated by QD1. The latter is always ferromagnetic in sign [39] and can bind a QD2-QD3 subsystem into a spin triplet. However, no matter how small t is, it always causes the antiferromagnetic exchange coupling of the resulting spin with the Fermi liquid formed by the Kondo screening at QD1. Therefore, at sufficiently cryogenic conditions, further Kondo screening occurs, which, with only one screening channel, results in the UK effect in the QD2-QD3 subsystem and spin-doublet ground state for the whole system. This is illustrated in Fig. 1(c), with CK screening cloud represented as in Fig. 1(b), and the more transparent shape illustrating the cloud corresponding to partial screening.

The picture presented so far is based on the assumption that the Kondo coupling of the first dot to the leads is sufficiently strong such that the interdot interactions do not give rise to the formation of molecularlike trimer states at temperatures above the Kondo temperature. However, with increasing t, the state depicted in Fig. 1(b) continuously evolves into the one schematically represented in Fig. 1(d). The latter no longer contains practically decoupled QD2-QD3 singlet. Instead, t correlates QD2 and QD3 with QD1, spreading the spin doublet from QD1 into the whole trimer. Nevertheless, for strong enough t', the tendency of antiparallel alignment guarantees that the trimer ground state would remain a spin doublet, which can be efficiently screened at sufficiently low temperatures by CK correlations.

Finally, for weak frustrating coupling t' and strong hopping t, the trimer acquires a magnetically staggered structure, with QD1 spin aligned antiparallelly to the spins of QD2 and QD3, which leaves the trimer in a spin doublet state. However, unlike for the strong t' case, now the coupling of the trimer to the leads is *ferromagnetic*, as the trimer spin direction follows the alignment of spins of QD2 and QD3 and is opposite to the direction of QD1 spin. In this way the FK system is formed, as sketched in Fig. 1(e).

As shown in the following, all these phases are vulnerable to the symmetry breaking introduced by the spin polarizations of the leads p. At nonzero temperatures, each phase splits into two regimes, separated by a crossover, with one comprising partially spin-polarized trimer stable in the low-temperature limit, and the other comprising nonmagnetized trimer, which is relevant only at elevated temperatures.

III. MODEL AND METHODS

The trimer coupled to the leads is modeled by a Hamiltonian of the general form $H = H_{\rm L} + H_{\rm R} + H_{\rm T} + H_{\rm 3QD}$, where the left (L) and right (R) leads are described by a single effective band [96], $H_{\rm L} + H_{\rm R} = \sum_\sigma \int \omega c^\dagger_{\omega\sigma} c_{\omega\sigma} {\rm d}\omega$, with $c^\dagger_{\omega\sigma}$ denoting the creation operator for an electron of energy ω and spin σ in a combination of relevant wave functions in respective electrodes coupled to the trimer. An effective hybridization is given by $\Gamma_\sigma(\omega) = \Gamma_{{\rm L}\sigma}(\omega) + \Gamma_{{\rm R}\sigma}(\omega)$ [96], so the tunneling Hamiltonian reads

$$H_{\rm T} = \sum_\sigma \int \sqrt{\frac{\Gamma_\sigma(\omega)}{\pi}} (c^\dagger_{\omega\sigma} d_{1\sigma} + {\rm H.c.}) {\rm d}\omega, \tag{1}$$

with $d^\dagger_{i\sigma}$ creating a spin-σ electron in QDi, $i = 1, 2, 3$. Note that only QD1 is coupled to the leads, cf. Fig. 1(a). We assume constant hybridization functions within the band of width $2D$, $\Gamma_{r\sigma}(\omega) = \Gamma_{r\sigma}(0)$ for $|\omega| < D$ ($\omega = 0$ at the Fermi energy), with sharp cutoff at energies $\pm D$. For the subsequent calculations, the magnetization of the leads (assumed parallel in the two leads) is represented by spin-dependent, left-right symmetric effective couplings, $\Gamma_{L\sigma} = \Gamma_{R\sigma} = \Gamma_\sigma = (1 + \sigma p)\Gamma/2$, with Γ measuring the coupling strength and p denoting the effective spin-polarization of the leads [83]. Assuming equal on-site repulsion U on each QD, the trimer Hamiltonian is written as

$$H_{\rm 3QD} = \sum_{i\sigma} \left(-\frac{U}{2} + \delta_i \right) n_{i\sigma} + \sum_i U n_{i\uparrow} n_{i\downarrow} + \sum_{i,j,\sigma} t_{ij} d^\dagger_{i\sigma} d_{j\sigma}, \tag{2}$$

where the summations run over $i, j \in \{1, 2, 3\}$ but $i \neq j$, $t_{ij} = t_{ji}$, and δ_i denotes the detuning of QDi from local particle-hole symmetry (PHS) point. The hoppings to two side-coupled QDs are assumed equal, $t_{12} = t_{13} = t$, while the frustrating coupling $t' = t_{23}$ is kept independent; see also Fig. 1(a).

To analyze the properties of this system, we use the NRG technique [29]. We construct the full density-matrix from states discarded during the calculation [97–99], and use an open-access code [100] as a basis for our implementation. This method allows us to reliably capture the full spectrum of the discretized Hamiltonian and calculate all the physical quantities directly from the spectral data, without any need for artificial broadening [101]. In particular, the linear conductance through the system at temperature T is calculated from [102]

$$G = \frac{e^2}{h} \sum_\sigma \int \left[-\frac{\partial f(\omega)}{\partial \omega} \right] \mathcal{T}_\sigma(\omega) {\rm d}\omega, \tag{3}$$

where $f(\omega)$ is the Fermi-Dirac distribution, and the spin-resolved transmission coefficient $\mathcal{T}_\sigma(\omega)$ is given in terms of the retarded Green's function of the first QD as

$$\mathcal{T}_\sigma(\omega) = -\Gamma_\sigma {\rm Im} \langle\langle d^\dagger_{1\sigma} | d_{1\sigma} \rangle\rangle(\omega). \tag{4}$$

The latter can be obtained in Lehmann representation directly from the NRG solution. The expectation values of the operators defined within the trimer subspace are obtained by taking the trace with the relevant reduced-density matrices [100,103].

To fully understand the nature of different Kondo phases, we also calculate the trimer contribution to the entropy. It can be found from

$$\mathbb{S}^{\rm imp} = \mathbb{S}^{\rm tot} - \mathbb{S}^0, \tag{5}$$

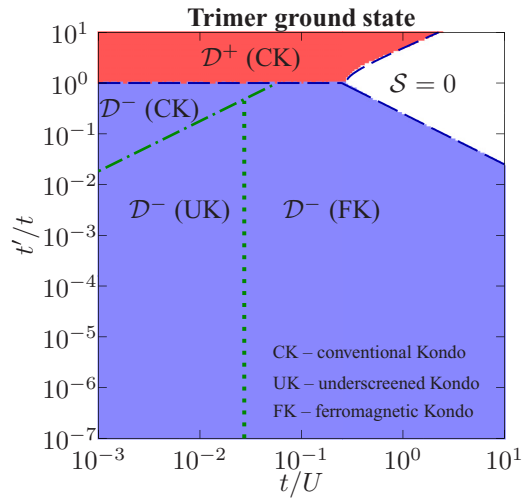

FIG. 2. The ground state of the isolated trimer for $\delta_i = 0$ and different t and t'. The violet (red) area corresponds to the odd-parity (even-parity) doublet ground state $\mathcal{D}^-$ ($\mathcal{D}^+$), while the white area corresponds to the singlet ground state $\mathcal{S} = 0$. In brackets, the expected phases that emerge in the presence of coupling to the leads are indicated, with schematic borders between them marked by dotted and dot-dashed lines. Details are explained in Sec. IV B.

where $\mathbb{S}^{\rm tot}$ denotes the entropy of the full system, whereas $\mathbb{S}^0$ is the entropy of the system without the trimer. The entropy is calculated directly from the spectrum of the discretized Hamiltonian (for a given set of parameters, one additional calculation is needed to determine $\mathbb{S}^0$).

Throughout the paper, we use the band cutoff as the energy unit, $D = 1$, and take the on-site repulsion U equal to the bandwidth, $U = D$, unless stated otherwise. The temperature is expressed in units of energy, i.e., the Boltzmann constant $k_B \equiv 1$. The lead spin polarization is assumed to be $p = 0.5$, yet the $p = 0$ case is also considered for comparison. The system is assumed to be at the local PHS point, $\delta_i = 0$; cf. Eq. (2). In the NRG calculations, we take the coupling strength to be $\Gamma = U/10$, the discretization parameter $\Lambda = 3$, and the number of states kept at each iteration is $N = 3000$.

IV. RELEVANT ENERGY SCALES

The most important low-temperature phases have been outlined in the discussion of Fig. 1. In the present section, we elaborate on them further, precisely explaining their origin. To determine the remaining phases, the phase boundaries between them and their fate at elevated temperatures, we discuss the relevant energy scales, in particular the exchange field $\Delta\varepsilon_{\rm ex}$ induced by the ferromagnetic leads. The results presenting the trimer's ground state and the exchange field as a function of hoppings t and t' are shown in Figs. 2 and 4. Then, the quantitative phase diagram is discussed in Sec. V and presented in Fig. 5.

A. Isolated trimer

We begin by considering the trimer decoupled from the leads. In general, we focus on regimes where the local Coulomb repulsion U is the largest energy scale. The phase diagram for such case is shown in Fig. 2. Even though $H_{\rm 3QD}$ can be in principle exactly diagonalized for $\delta_i = 0$, the solution involves roots of a general quartic polynomial and is not very insightful. However, we find it important to note that for $\delta_i = t' = 0$ the trimer Hamiltonian $H_{\rm 3QD}$, Eq. (2), exhibits the PHS defined by the simultaneous transformation on all the QDi's ($i = 1, 2, 3$), $d_{i\sigma} \mapsto s_i d^\dagger_{i\sigma}$, provided the coefficients s_i are all of module 1 and $s_2 = s_3 = -s_1$. However, even for $\delta_i = 0$, the term proportional to $t' \equiv t_{23}$ changes sign upon this transformation and inevitably destroys this symmetry. Therefore, despite the assumed local PHS at each site of the trimer, the global PHS is not preserved, and the trimer may not even be half filled in the ground state.

Insight into the energy spectrum of the trimer can be obtained based on the observation that, as long as $\Gamma = 0$, one can use U^{-1} as a small expansion parameter. One immediately sees that there are only eight states of energy of the order of $-3U/2$, which are separated from the other states by energy differences of at least $\sim U/2$. Therefore, these are the states important for the low-temperature physics in all the Kondo regimes. Actually, four of them form a symmetry-preserved spin quadruplet of energy $E_{\mathcal{S}=3/2} = -3U/2 + \delta_1 + \delta_2 + \delta_3$. The remaining states form two $\mathcal{S} = 1/2$ doublets (which are coupled to other doublets of energy by at least $\sim U$ higher). The two low-energy eigenstate doublets, denoted by $\mathcal{D}^+$ and $\mathcal{D}^-$, are actually always lower in energy than the quadruplet and have even ($\mathcal{D}^+$) or odd ($\mathcal{D}^-$) parity with respect to exchange of QD2 with QD3, respectively. For $t' = 0$, the ground state is the odd-parity doublet $\mathcal{D}^-$. Increasing the frustration brought about by t' causes a level-crossing QPT at $t' = t$, as illustrated by the colored regions in Fig. 2 (note the logarithmic scales on both axes and the t'/t normalization on the vertical axis). For low values of $t < U/10$ and $t' < t/20$, the energy difference $E^* = |E^+_{S=1/2} - E^-_{S=1/2}|$ of these two doublets is of the order of the exchange coupling between the relevant QDs:

$$E^* \approx \frac{4t^2}{U}|1 - t'/t|^2. \tag{6}$$

Thus, one should expect these two phases to become indistinguishable for temperatures $T \gtrsim E^*$.

Finally, as can be seen in Fig. 2, when the interdot hopping becomes large in comparison to local Coulomb repulsion, $t, t' \gtrsim U/4$, an additional phase is present, labeled $\mathcal{S} = 0$. This is a spinless state, occupied (for positive t') with four electrons. Its presence is a clear manifestation of the lack of the global PHS in the model (even in the presence of the local one), which is caused by the frustrating coupling t'. Nevertheless, this singlet is present even without coupling to the leads. It is, therefore, not a Kondo state and will not be discussed in detail in the present paper.

B. The Kondo scales

When the trimer is coupled to the leads, the most important observation concerns the effective exchange coupling of the two doublets relevant at the lowest temperatures [38]. The even doublet, $\mathcal{D}^+$, is coupled in a conventional antiferromagnetic manner, with the same strength as the QD1 spin itself, $J^{\rm CK} = 8\Gamma/(\pi\rho U)$, ($\rho$ denotes the normalized density of leads

states at the Fermi level). This means that no matter how weak this coupling is, whenever temperature drops below the Kondo temperature T_K, the trimer spin $\mathcal{S} = 1/2$ is fully screened by the electrodes due to the CK effect. Hence the CK label in Fig. 2. The relevant value of T_K can be estimated on the basis of the Anderson's poor man's scaling method [55], even for finite lead spin polarization p [104,105], to give

$$T_K = \sqrt{\frac{\Gamma U}{2}} \exp\left[-\frac{\pi}{8}\frac{U}{\Gamma}\frac{\operatorname{atanh}(p)}{p}\right]. \tag{7}$$

For $\Gamma = U/10$ used throughout the paper, one gets $T_K(p{=}0.5) \approx 0.003U$ and $T_K(p{=}0) \approx 0.0044U$.

Meanwhile, the odd-parity doublet $\mathcal{D}^-$ is coupled ferromagnetically, although with reduced strength. Namely, $J^{\mathrm{FK}} = -J^{\mathrm{CK}}/3$ [38]. Therefore, the FK effect is expected, see Fig. 2, which leads to asymptotically free spin [55] and singular dynamics [56] at low temperatures. Due to the fact that the exchange coupling is inevitably proportional to Γ, this gives the characteristic temperature scale $\widetilde{T}_K$ following Eq. (7) with Γ replaced by $\Gamma/3$. For $\Gamma = U/10$, this gives $\widetilde{T}_K(p{=}0.5) = 3.09 \times 10^{-7}U$ and $\widetilde{T}_K(p{=}0) = 9.87 \times 10^{-7}U$. Note, that for both two cases of $p = 0$ and $p = 0.5$, $\widetilde{T}_K \ll T_K$. Therefore, one expects that in the temperature regime of $\widetilde{T}_K < T < T_K$ the Kondo effect takes place at QD1 only, despite quite strong t. This is confirmed by NRG calculations presented in Sec. VI.

Since the ground states corresponding to CK and FK regimes differ in spin quantum number, they are separated by the QPT. Nevertheless, it does not occur exactly for $t' = t$. In fact, since J^{CK} scales up and J^{FK} scales down with decreasing temperature, it is hardly surprising that the CK phase takes over the FK phase for $t' = t$ and the QPT line moves to $t' \equiv t'_c < t$, where t'_c denotes the transition point between the CK and FM phases, yet roughly independent of t. Nevertheless, even for couplings as strong as $\Gamma = U/10$ the difference between t'_c and t occurs to be hardly noticeable, cf. NRG results in Sec. VI.

However, the above considerations contain an implicit assumption that the molecular trimer orbitals are still well-defined for $\Gamma > 0$. This seems reasonable if the inter-QD exchange interactions are large in comparison to T_K, $J_2 \approx 4t^2/U \gtrsim T_K$. If, on the contrary, $t \lesssim \sqrt{UT_K}/2$, then at temperatures below T_K, yet above some critical value of the order of J_2, single electrons occupying QD2 and QD3 are not correlated with QD1 due to thermal fluctuations, while QD1 spin is almost fully screened by CK effect, therefore, forming a Fermi liquid state [54]. The characteristic value of t, around which the crossover happens, shall be denoted as

$$t_x = \tfrac{1}{2}\sqrt{T_K U}. \tag{8}$$

The second and third dot (QD2 and QD3) spins may still be correlated with each other though, if the hopping-induced antiferromagnetic exchange interaction $J_2{}' \sim 4(t')^2/U$ exceeds temperature fluctuations. When the temperature falls further, a superexchange also comes into play, mediated by QD1-and-leads quasifree pseudoparticles. The latter has a ferromagnetic sign and a magnitude of the order of $J_{\mathrm{SX}} \sim t^2/\sqrt{T_K U}$ [39]. The interplay between J_{SX} and J'_2 (which is in fact a competition between t and t' again) determines the state of the QD2-QD3 cluster to be either the spin singlet, depicted in Fig. 1(b), or $\mathcal{S} = 1$ triplet, cf. Fig. 1(c). The position of the transition anticipated from $J'_2 = J_{\mathrm{SX}}$ criterion is marked in Fig. 2 with a dot-dashed line.

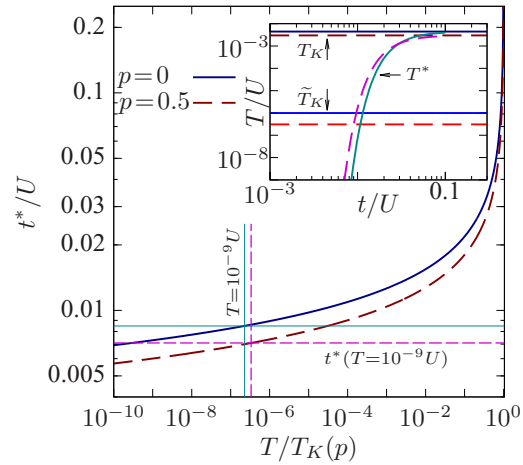

FIG. 3. The dependence of the critical hopping t^* on temperature based on Eq. (10) calculated for $\Gamma = 0.1U$ in the case of nonmagnetic ($p = 0$) and magnetic leads ($p = 0.5$). In the inset, all the relevant Kondo scales are plotted against the hopping t. More details are provided in the main text of Sec. IV B.

The story of the former case is already finished, as this is a stable low-temperature state, actually a special case of the CK state discussed so far. Yet, the fate of the triplet state is still not concluded. In fact, in the case of formation of $\mathcal{S} = 1$ within the QD2-QD3 cluster, lowering the temperature further gives rise to another Kondo screening. Indeed, the QD1-and-leads Fermi liquid screens the QD2-QD3 spin at temperatures of the order of [106]

$$T^*(t) = \alpha T_K \exp(-\beta T_K U/4t^2), \tag{9}$$

as the local density of states of QD1, exhibiting the Kondo peak of the width $\sim T_K$, serves as a band for QD2-QD3 cluster. The coefficients α and β are of the order of unity and depend on the system parameters weakly, see also Ref. [106]. The dependence of $T^*(t)$ for $\Gamma = U/10$ and $p \in \{0, 0.5\}$ is plotted in the inset in Fig. 3; the (t-independent) values of T_K and $\widetilde{T}_K$ are indicated there as well. However, the screening of $\mathcal{S} = 1$ cannot be complete with only one screening channel, therefore it is underscreened in the sense of Nozieres-Blandin Fermi-liquid theory [57]. Hence, we call this regime the UK regime, see Fig. 2. It seems noteworthy that this phase has all the quantum numbers identical to the FK phase, discussed earlier, including the residual $\mathcal{S} = 1/2$ spin in the ground state. In fact, these phases are continuously connected both for $p = 0$ [39] and $p > 0$; see Sec. VI. The estimation of the position of the UK/FK crossover based on $4t^2/U = T_K$ criterion for $\Gamma = U/10$ and $p = 0.5$ is indicated in Fig. 2 with a dotted line.

Importantly, T^* given by Eq. (9) is very low for weak t', so at some temperature $T > 0$, there exists such a critical value of t, denoted $t^*(T)$, that $T^*[t^*(T)] = T$. In fact, taking $\alpha \approx \beta \approx 1$, we find from Eq. (9):

$$t^*(T) \approx \frac{1}{2}\sqrt{\frac{T_K U}{\ln(T_K/T)}}. \tag{10}$$

Estimating the Kondo temperature from Eq. (7), for $\Gamma = 0.1$ and $p = 0.5$, one can calculate t^* for experimentally relevant temperatures and make clear that in practice for $t^* < 0.005U$ the non-zero temperature regime is experimentally relevant, see Fig. 3.

As explained earlier, the transition point between the CK and FK phases, t_c', remains practically independent of t and close to $t' = t$. However, this is no longer the case in the UK regime, where the transition is strongly shifted to [39]

$$t_c' \approx \frac{t^2}{\sqrt{T_K U}}, \tag{11}$$

which is particularly small for weak t. This estimation of transition point is indicated in Fig. 2 by the dot-dashed line. Note that due to the dependence of the Kondo temperature on spin polarization p, the critical value t_c is a function of p as well. Furthermore, due to the fact that the UK and FK phases are separated by a continuous crossover only, it is sensible to continue the line to the transition position characteristic of the FK regime.

C. The exchange field

In general, the coupling between a nanodevice and the leads gives rise to the renormalization of the energy levels of the nanodevice. In the case of magnetic leads, this renormalization is usually spin dependent [83]. The part of its linear contribution proportional to leads magnetization p is often called the (spintronic) exchange field and will be denoted $\Delta\varepsilon_{\rm ex}$ [107]. For single impurity, $\Delta\varepsilon_{\rm ex}$ is altered smoothly while lifting impurity energy level, changing sign at the local PHS point. However, in the trimer case PHS is broken by the frustration, and $\Delta\varepsilon_{\rm ex}$ no longer vanishes even at local PHS, opening the possibility for spin polarization of the nanostructure in such conditions. It is noteworthy that at sufficiently small temperatures, even very small value of frustrating hopping t' may result in substantial magnitude of $\Delta\varepsilon_{\rm ex}$. In the present section, to obtain certain insight into the properties of $\Delta\varepsilon_{\rm ex}$ in the case of a locally PHS trimer, we performed a perturbative analysis. However, these predictions will be corroborated further in Sec. VI by accurate NRG calculations.

For each eigenstate of the isolated trimer $|e_i\rangle$, the shift of its energy E_i due to interaction with ferromagnetic leads is linear in p in the leading (second) order of perturbation theory in the hopping matrix elements between the trimer and the leads. Within the wide-band limit discussed in Sec. III, the exchange field in that state is, therefore, defined as [107]

$$\Delta\varepsilon_{\rm ex}^i = \sum_{j\sigma} \frac{\sigma p\Gamma}{\pi\langle e_i|\hat{\mathcal{S}}_z|e_i\rangle} \ln\left|\frac{E_j - E_i}{D + (E_j - E_i)}\right| \times\left(|\langle e_j|d_{1\sigma}^\dagger|e_i\rangle|^2 + |\langle e_j|d_{1\sigma}|e_i\rangle|^2\right), \tag{12}$$

where the spin index σ is understood as ± 1 when factoring numbers and $\hat{\mathcal{S}}_z$ denotes the operator of zth component of trimer spin. This is a proper definition for $\langle e_i|\hat{\mathcal{S}}_z|e_i\rangle \neq 0$, yet for spinless states the right-hand side of the equation vanishes anyway and $\Delta\varepsilon_{\rm ex}^i$ can be set arbitrarily. The convenient choice is to put it to the mean over the values within the multiplet for $\mathcal{S} > 0$ states and to 0 for $\mathcal{S} = \mathcal{S}_z = 0$. In fact, the structure of the low-energy spectrum presented in Sec. IV A, i.e., spin quadruplet and two spin doublets, is preserved within this definition, namely, $\Delta\varepsilon_{\rm ex}^i$ is the same for all states within each multiplet (but differs between multiplets).

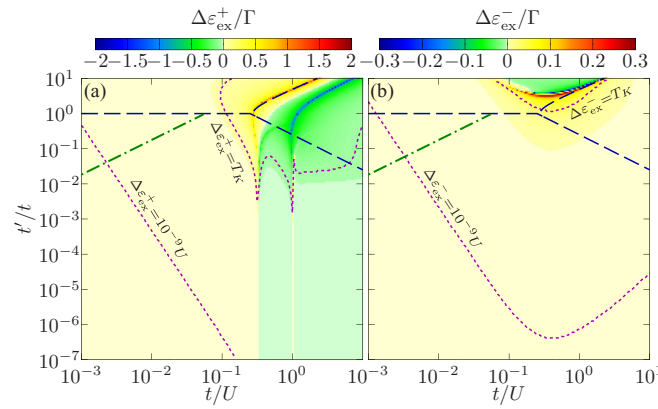

FIG. 4. (a) The exchange field in the even-parity doublet state $\mathcal{D}^+$, calculated within perturbation theory for $U = D$ and $p = 0.5$. (b) Similar plot of the exchange field in the odd-parity doublet state $\mathcal{D}^-$. Note the logarithmic scales on both axes in all plots. More details are provided in the main text of Sec. IV C.

The exchange fields in the two relevant doublet states, $\mathcal{D}^+$ and $\mathcal{D}^-$, denoted correspondingly $\Delta\varepsilon_{\rm ex}^+$ and $\Delta\varepsilon_{\rm ex}^-$, are presented in Figs. 4(a) and 4(b) for a trimer at the local PHS point in a wide range of t and t'. This wide range of hopping constants allows for making predictions for different possible realization of the trimer, including molecules as well as QD systems. Note in particular, that the smallest used value of t', $t'/t = 10^{-7}$, is already a value one can expect for a next-nearest-neighbor interaction strength in a linear molecule.

The dashed and dot-dashed lines shown in Figs. 4(a) and 4(b) are the same as those in Fig. 2 and indicate the positions of the QPTs. The first observation is that in the regimes where the scale comparison suggests the CK ground state, i.e., where $\mathcal{D}^+$ is the most relevant state, $\Delta\varepsilon_{\rm ex}^+ > 0$. Similarly, wherever the UK or FK ground state is expected, $\Delta\varepsilon_{\rm ex}^- > 0$, while the exchange field in the spinless ground state obviously vanishes, $\Delta\varepsilon_{\rm ex}^{\mathcal{S}=0} = 0$. Therefore, one expects that at local PHS (assumed for the calculation) the exchange field in the states relevant at low T is non-negative, $\Delta\varepsilon_{\rm ex} \geqslant 0$. This is in agreement with transport properties calculated with NRG in Sec. VI. Moreover, one also expects that whenever the ground state of the system is not a spin singlet, $\Delta\varepsilon_{\rm ex}$ would split the ground state spin degeneracy and lead to states comprising a spin polarized trimer. This should be expected in particular in the FK and UK phases, which from now on will be denoted as FK$'$ and UK$'$, when the doublet degeneracy is lifted. Furthermore, $\Delta\varepsilon_{\rm ex} > T_K$ may split the Kondo resonance in the CK phase [83,105]. In the following, this resulting regime will be denoted as CK$'$. In other words, the different regimes in the case of magnetic leads will be denoted with a prime.

One easily notes that $\Delta\varepsilon_{\rm ex}$ is in general quite small, except for the regions where two relevant states are close to degeneracy, since then the denominator in Eq. (12) blows up. However, as this is only a perturbative expression, one

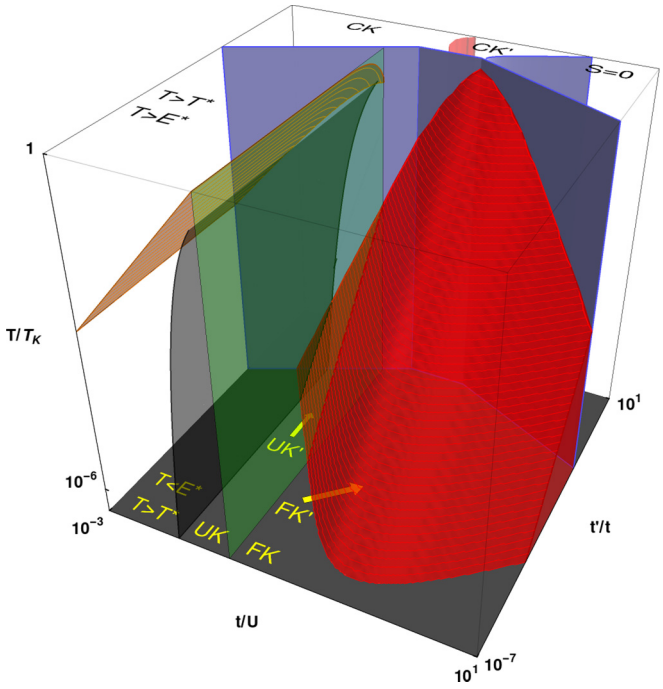

FIG. 5. Schematic phase diagram of the considered system for $T \leqslant T_K$ and for magnetic leads with spin polarization $p = 0.5$ calculated vs the following parameters: the hopping t (in units of Coulomb repulsion U), the frustrating coupling t' (normalized by t), and the temperature T (scaled by T_K). Note the logarithmic scale of all the axes. The respective phases are described in the main text of Sec. V.

should take that result with a lot of caution. Even though some enhancement of trimer energy levels renormalization is expected there, one does not, in general, expect them to be divergent, even in the $T \to 0$ limit. Indeed, note that NRG results presented in Sec. VI indicate regular behavior of the trimer magnetization.

Finally, from Figs. 4(a) and 4(b), it is evident that the exchange field in the ground state, $\Delta\varepsilon_{\rm ex}^{\rm GS}$, apparently has quite a small absolute value. To make it even more clear, we added dotted lines in both figures to indicate where the exchange field is equal to the conventional Kondo scale, $\Delta\varepsilon_{\rm ex}^{\rm GS} = T_K$, and where it equals $10^{-9}U$. The latter is intended to mimic the zero-temperature regime. Clearly, even at such a small T, not all of the considered parameters $|\Delta\varepsilon_{\rm ex}^{\rm GS}| > T$ are expected. This is an important feature for the phases of trimer in all temperature regimes. In particular, one can expect that the phases FK′ and UK′ are possible only when $T < \Delta\varepsilon_{\rm ex}$, while at elevated temperatures the nonmagnetized FK and UK regimes should be expected.

V. THE OVERVIEW OF THE PHASE DIAGRAM

The three-dimensional phase diagram of the trimer, featuring t, t', and T as parameters, is presented in Fig. 5. Already, the first sight of it allows us to realize that it is fairly complicated, however, the analysis of energy scales performed in the preceding section shall allow us to identify and understand all the phases.

We start the discussion from the QPT lines introduced as dashed or dot-dashed lines in Fig. 2. They are presented as solid vertical walls, without any broadening for elevated temperatures for the sake of clarity of the figure. Their positions are based on the exact positions of ground-state changes for the isolated trimer for $t > \sqrt{T_K U}$ and given by Eq. (11) for smaller t. The transparent vertical wall is used to indicate the position of the crossover between UK and FK phases, which is quite arbitrarily defined to be at $t = t_x$, fulfilling Eq. (8).

In turn, we move to the discussion of nonzero T properties of the UK phase. As explained in Sec. IV B, the second Kondo temperature is indeed cryogenic for small t. The approximate position of the crossover between partially screened and unscreened $\mathcal{S} = 1$ QD2-QD3 cluster is indicated in Fig. 5 by the dark opaque leaning surface, based on Eq. (10). Even though the bottom of the figure corresponds to $T = 10^{-9}U < 10^{-6}T_K$, the uttermost left part of the figure still corresponds to the $T > T^*$ regime, which vanishes only in the purely mathematical $T \to 0$ limit. On the other hand, further increase of T inevitably leads to the next crossover, occurring when the thermal energy reaches the excitation energy between the two relevant eigenstate doublets, $T = E^*$. Above this threshold, the states at two sides of the transition are similarly probable and the physical properties are expected to be a mean of the properties of each of them. In particular, the $\mathcal{S} = 1$ state is not fully formed within the QD2-QD3 cluster. Additionally, note that E^* is estimated by Eq. (6), however, one needs to remember that this formula does not take into account the shift of the UK/CK QPT away from $t' = t$, therefore it overestimates E^* very close to that transition. Nevertheless, this estimation is sufficient for qualitative understanding of the phases of the system and is used to plot the crossover position as a skewed surface in the phase diagram in Fig. 5.

It is noteworthy to point out that all phases discussed so far exist also for $p = 0$. However, some changes in position of borders occur then, because of the difference between (lower) $T_K(p{=}0.5)$ and (higher) $T_K(p{=}0)$, cf. Eq. (7). Therefore, for example, t_c' is somewhat smaller for $p = 0$, as follows from Eq. (11). Similarly, t^* is larger for $p = 0$, cf. Fig. 3.

Another way to obtain interesting spintronic properties is to exploit the unique features present only for $p > 0$. They are in general caused by the presence of the exchange field in the ground state, $\Delta\varepsilon_{\rm ex}^{\rm GS} \neq 0$. First, the exchange field suppresses the CK effect if $\Delta\varepsilon_{\rm ex} \gg T_K$ and splits the Kondo peak in QD1 spectral density for $\Delta\varepsilon_{\rm ex} \approx T_K$. In both cases, one expects QD1 to become spin polarized, even though at local PHS (as considered here) the global PHS is broken actually only by the t' hopping between QD2 and QD3. Therefore, one can see the coupling to the QD2-QD3 cluster as a kind of functionalization of QD1-based device. These magnetic phases are separated from basically nonmagnetic states for $\Delta\varepsilon_{\rm ex}^{\rm GS} \ll T_K$ by a continuous crossover, as is for the case of a single QD outside of the PHS point [83,105], indicated in Fig. 5 with a curved vertical wall, with magnetic phase labeled as CK′ and the nonmagnetic simply by CK on the top face of the diagram.

Furthermore, one can predict an even more pronounced effect of the exchange field at the FK side of the transition. There, not only is the relevant Kondo scale much smaller, but also the ground state comprises an asymptotically free spin doublet, so at sufficiently low temperatures the exchange field

always overcomes the ferromagnetic coupling to the leads. Therefore, in the $T \to 0$ limit only the phase with nonzero dot magnetization, denoted FK$'$, is stable. However, as discussed in Sec. IV C, the magnitude of the exchange field is actually very small for small t and t', so at finite temperatures the region where the thermal fluctuations do not overcome $\Delta\varepsilon_{\rm ex}^{\rm GS}$ is finite, compare dashed lines in Figs. 2 and 4. This gives rise to the crossover between the magnetic phase FK$'$ and the nonmagnetic FK phase at $T = \Delta\varepsilon_{\rm ex}^{\rm GS}$, which is indicated in Fig. 5 with a striped domelike surface. Note also that dotted lines labeled as $\Delta\varepsilon_{\rm ex}^{-} = 10^{-9}U$ in Fig. 4(b) signify in fact the footprint of the FK$'$ phase on the "floor" of the diagram, corresponding to $T = 10^{-9}U$.

Both FK and FK$'$ phases continue through the described earlier crossover toward the UK (and correspondingly the magnetic UK$'$) phase, where, additionally, an effective $\mathcal{S} = 1$ state is formed within the QD2-QD3 cluster. This is a particularly interesting state, as here QD1 in fact experiences CK, yet still in partially screened QD2-QD3, the magnetic order is imposed, with $\mathcal{S} = 1$ almost fully aligned with lead minority spins for temperatures both below T^* and above it. This is the case as long as the temperature does not overcome the effective ferromagnetic coupling between the second and third QDs.

VI. NUMERICAL RESULTS

In this section, we present the results of NRG calculations concerning the physical properties representative for each Kondo regime of the system. These include the linear conductance G and the expectation value of the trimer spin $\mathcal{S}$, the trimer's spin polarization, as well as the trimer's entropy. The studied quantities clearly confirm the predictions of the qualitative analysis performed in Secs. IV and V.

A. Conductance

The unitary conductance through the device is possibly the most well-known hallmark of the CK state for nonmagnetic leads, $G = G_0 = 2e^2/h$. The conductance possesses this value in the CK regime and in the $T > T^*$ part of the UK regime, see Fig. 6(a). On the contrary, it abruptly changes at the QPT between the CK and FK phases, while changing continuously with increasing t from the UK to the FK phase. In agreement with earlier predictions, at the CK side of the transition, the conductance remains maximal while increasing t up to the transition point to the $\mathcal{S} = 0$ phase, where it ultimately vanishes. Notably, for $p = 0$, there is hardly any t' dependence of the conductance for $t' < t'_c$.

The latter is no longer true for $p > 0$. It is clearly visible in Fig. 6(b) that in the FM$'$ region [whose border is indicated with a dashed line, similarly to Figs. 4(a) and 4(b)], the conductance depends on t', and is in particular larger than for $p = 0$. This trend persists also at higher T, cf. Fig. 6(c). However, for sufficiently large temperatures, the FM$'$ region is practically not present; see Fig. 6(d). Meanwhile in the CK regime for $p = 0.5$, $G = G_0$ and is reduced after crossover to the CK$'$ phase driven by increasing t. This remains true as long as $T \ll T_K$, as visible in Figs. 6(b) and 6(c). However, since $T = 10^{-3}U$ is already close to T_K, the conductance in the CK phase drops in this case below G_0 and decreases even further in the CK$'$ regime.

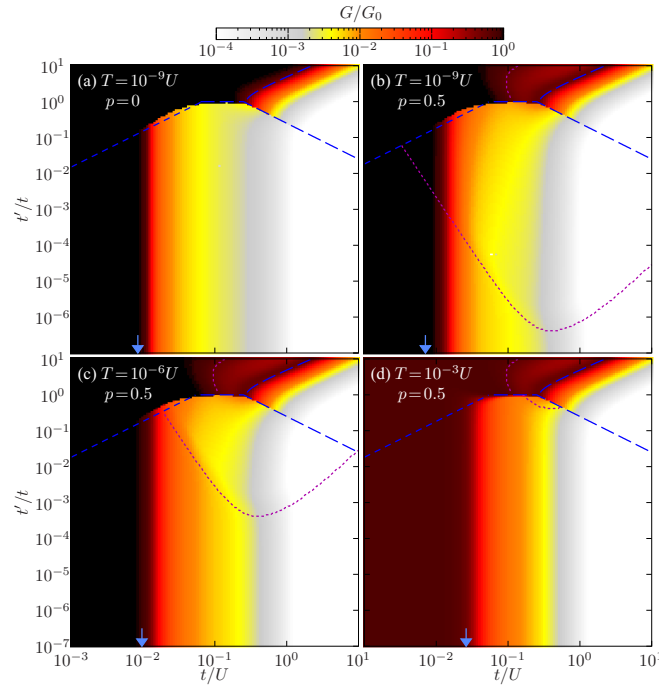

FIG. 6. Conductance as a function of t and t' for $\Gamma = 0.1U$, $\delta_i = 0$, and for (a) $T = 10^{-9}U$ and $p = 0$ (b)–(d) finite spin polarization $p = 0.5$ and different temperatures indicated in the figure. Dashed lines correspond to boundaries of phases from Figs. 2 and 5. Arrows indicate $t = t^*$ points on vertical axes according to Eq. (10). Note the logarithmic color scale.

B. Spin expectation value

In the behavior of the conductance, it is not possible to see the difference between the CK and UK phases in the regime of $t < t^*$. Therefore, we now analyze the expectation value of the trimer spin, defined as such a scalar $\mathcal{S}$ that the expectation value of the operator of trimer squared spin, $\hat{\mathcal{S}}^2_{\rm 3QD}$, fulfills

$$\mathcal{S}(\mathcal{S}+1) = \langle \hat{\mathcal{S}}^2_{\rm 3QD} \rangle. \tag{13}$$

This definition allows us to talk about *trimer spin* as a continuous quantity, in principle having values in the range $\{0 \leqslant \mathcal{S} \leqslant 3/2\}$. Note that Kondo screening of the local moment does not lead to screening of the spin in terms of the definition given by Eq. (13). This is because the leads states (also these screening local spins) are averaged out when calculating the expectation value. Therefore, $\mathcal{S}$ quantifies the magnitude of the spin screened in the Kondo phase, rather than the degree of screening.

1. Conventional Kondo (CK) regime at low temperatures

Keeping that in mind, for low temperatures, one expects in particular $\mathcal{S} \approx 1/2$ in the CK phase. However, as one can see in Figs. 7(a) and 7(b), the CK phase value of $\mathcal{S}$ is in fact somewhat smaller than $1/2$ and close to $\mathcal{S} = 0.45$. This is because for large t', the QD2-QD3 effective exchange has an antiferromagnetic nature and the charge fluctuations are

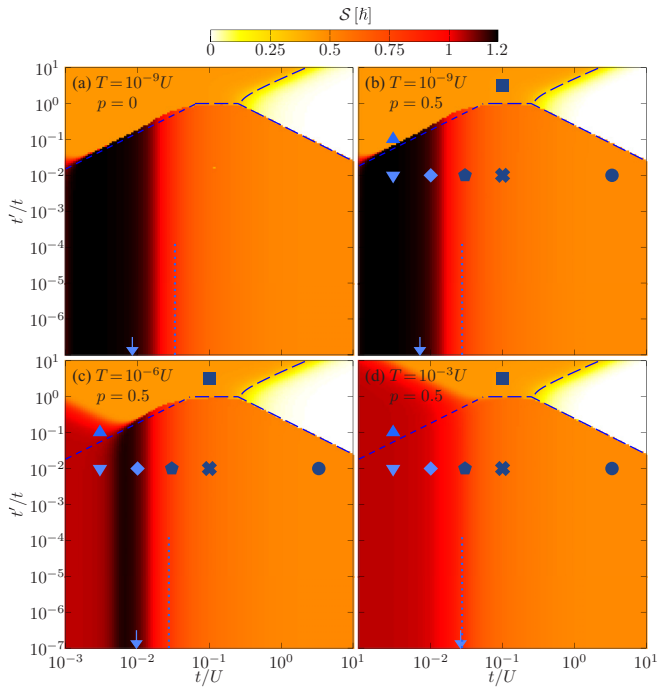

FIG. 7. The expectation value of the trimer spin $\mathcal{S}$ as a function of t and t'. The parameters are the same as in Fig. 6. The points marked with symbols indicate t and t' for which Fig. 8 is prepared. Small vertical arrows (dotted lines) indicate t^* (t_x) positions, correspondingly.

more likely to cause the $\mathcal{S}=0$ state to be an intermediate state [with empty QD1 and QD2-QD3 in a singlet state, cf. Fig. 1(b)] than the $\mathcal{S}=1$ state [cf. Fig. 1(c)]. This is indeed confirmed in Fig. 7(a) for $p=0$ and in Fig. 7(b) for $p=0.5$, see in particular the points indicated by the square and the upturned triangle in the latter. Apparently, except for very small changes in the positions of phase boundaries, the degree of spin polarization p is pretty much irrelevant for the spin expectation values (this is obviously not true for $\mathcal{S}_z$, see Sec. VI C).

2. Conventional Kondo phase at higher temperature

The temperature dependence of $\mathcal{S}$ for t and t' corresponding to these two points is presented in Fig. 8 with dashed lines and adequate symbols. One clearly sees that for $t=0.1U$ and $t'=3t$ (square) $\mathcal{S}(T)$ remains constant up to $T\sim\Gamma$, while for $t=0.003U$ and $t'=0.1t$ (up-turned triangle) the spin-expectation value already rises for $T\sim 10^{-5}\,T_K$. The latter is caused by the fact that internal trimer exchange couplings and the excitation energy E^* are all very small for weak t and t', cf. Eq. (6) and the discussion following Eq. (8). Therefore, for $T>E^*$, the magnetic correlations between the individual QDs become irrelevant and all the states comprising singly occupied dots are almost equally probable. There are eight such states, forming two $\mathcal{S}=1/2$ doublets and a single $\mathcal{S}=3/2$ quadruplet, thus for $E^*\ll T\ll U$ we have $\langle\hat{\mathcal{S}}^2_{3\mathrm{QD}}\rangle=9/4$ and hence the universal middle-temperature value for small values of t and t' is $\mathcal{S}=\sqrt{5/2}-1/2\approx 1.08$. As seen in Fig. 8, in reality it is somewhat smaller due to the residual correlations, nevertheless Figs. 7(c)–7(d) show how wide the range of

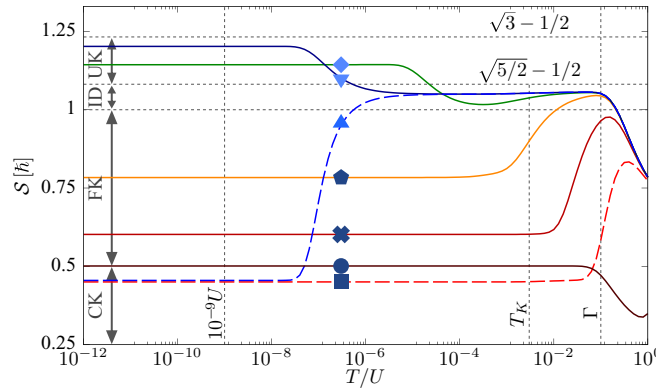

FIG. 8. The trimer spin expectation value $\mathcal{S}$ as a function of T for values of t and t' indicated in Figs. 7(b) and 7(d) with corresponding symbols. The other parameters are the same as in Fig. 7. See Sec. VI B for details.

parameters is where this formula holds. Note, however, that while QDs are not correlated among themselves, QD1 may still be Kondo screened by the leads.

3. Underscreened Kondo (UK) phase

Clearly, the $\mathcal{S}\approx\sqrt{5/2}-1/2$ region includes states also belonging to the UK phase at temperatures above E^*, i.e., when the effective $\mathcal{S}=1$ state is not yet formed in the QD2-QD3 cluster; see the lines denoted by a down-turned triangle and a pentagon in Fig. 8 and their positions in Figs. 7(b)–7(d). However, at low temperatures $\mathcal{S}$ approaches another quite universal value, $\mathcal{S}\approx\sqrt{3}-1/2\approx 1.23$. Again, the true maximum is slightly smaller, see the corresponding lines in Fig. 8, but the increase from below $\mathcal{S}\approx\sqrt{5/2}-1/2$ is clearly visible. This value can also be understood as characterizing the trimer comprising QD2 and QD3 forming a spin triplet and QD1 forming a spin-doublet state. Averaging over possible zth component configurations gives $\langle\hat{\mathcal{S}}^2_{3\mathrm{QD}}\rangle=11/4$, i.e., $\mathcal{S}=\sqrt{3}-1/2$. Therefore, this value (slightly decreased by remaining correlations) is characteristic of the UK phase.

4. Ferromagnetic Kondo (FK) phase

Since the UK phase is separated from the FK phase only by the crossover, the value of $\mathcal{S}$ decreases continuously toward $\mathcal{S}=1/2$ with increasing t. However, opposite to the CK phase, the residual QD2-QD3 correlations are ferromagnetic in this regime, therefore, the final value $\mathcal{S}\gtrsim 1/2$, as can be seen in Fig. 8 for the curves marked with a pentagon, cross, and a circle.

5. Summary of the section

In summary, the spin expectation value $\mathcal{S}$ defined in Eq. (13) is an excellent marker of the phases, capable of differentiating between all the relevant regimes, especially these having similar transport properties. It reaches the highest values $\mathcal{S}\lesssim\sqrt{3}-1/2$ in the UK phase (both below and above T^*). It is reduced below $\mathcal{S}\approx\sqrt{5/2}-1/2$ in the regime of almost independent, but singly occupied QDs and decreases continuously toward $\mathcal{S}\gtrsim 1/2$ in the FK phase. The QPT between the FK and CK regions is marked by an abrupt jump

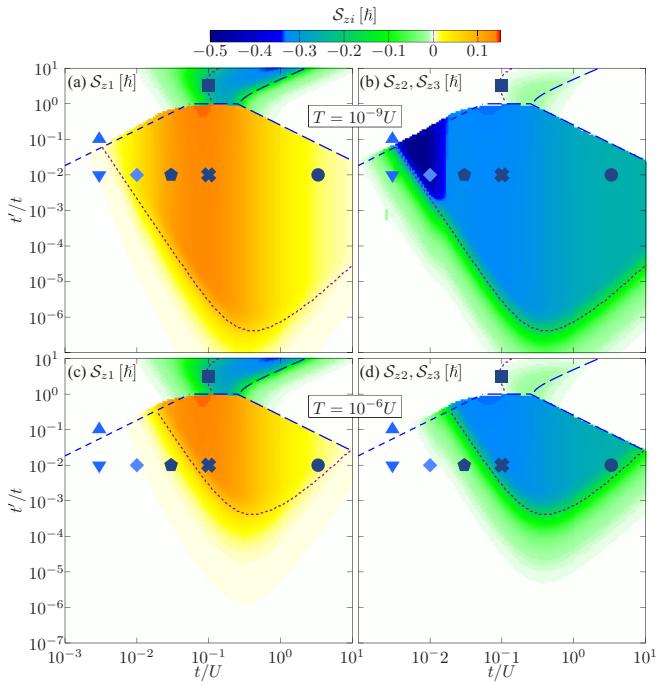

FIG. 9. The z component of spin of respective quantum dots as functions of t and t'. Parameters are the same as in Fig. 6 with $p = 0.5$. Dotted lines indicate where the condition $\Delta\varepsilon_{\rm ex}^{\rm GS} = T$ (in the UK or FK phase) or $\Delta\varepsilon_{\rm ex}^{\rm GS} = T_K$ (in the CK regime) is fulfilled. Symbols have the same positions as in Fig. 7.

of $\mathcal{S}$ to some value $\mathcal{S} \lesssim 1/2$ on the CK side of the transition. Finally, the spinless trimer phase, scarcely discussed here, is characterized by $\mathcal{S} = 0$. $\mathcal{S}$ does not change due to the Kondo screening, yet its presence or absence in each phase can be recognized from the value of the conductance, as explained in the preceding section and visible in Fig. 6. The nature of different phases is further confirmed in Sec. VI D by the calculations of the trimer's entropy. However, the spin expectation value does not allow for distinguishing the polarized phases from their nonpolarized counterparts, i.e., CK from CK′, FK from FK′, and UK from UK′. Therefore, there is one additional quantity one needs to pinpoint all the phases within NRG framework, namely, the trimer spin polarization. The related results are presented in Sec. VI C.

C. Trimer spin polarization

An important consequence of the existence of the exchange field is the spin polarization of the trimer, quantified by the expectation value of the spin of respective QDs, denoted $\mathcal{S}_{zi}$ for QDi. As can be seen in the left column of Fig. 9, $\mathcal{S}_{z1} \neq 0$ in the UK and FM phases, as long as the condition $T < \Delta\varepsilon_{\rm ex}^{\rm GS}$ is fulfilled. It seems noteworthy that $|\mathcal{S}_{z1}|$ does not reach $\pm 1/2$, yet the values are typically of the order of $1/10$, even for very small values of frustrating coupling t'; cf. Fig. 10. In fact, in the $T \to 0$ limit $\mathcal{S}_{z1} \neq 0$, in the whole UK and FK regimes for any nonzero t'. This is in contrast to the case of a single QD slightly detuned from the PHS. Then, the QD spin polarization is proportional to the symmetry-breaking detuning. It also means that the ground state always belongs to

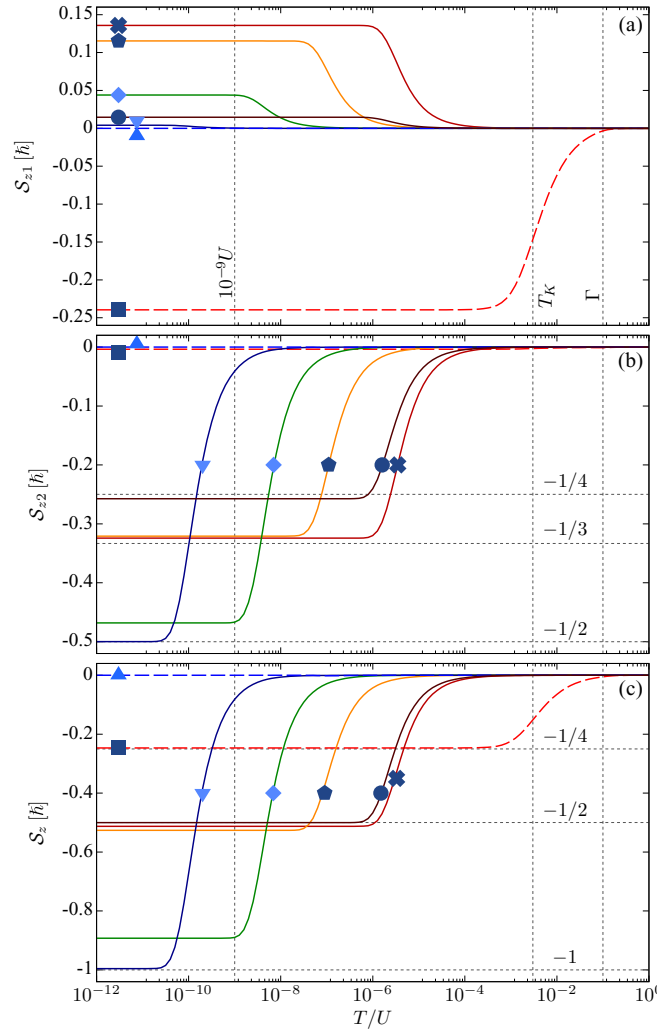

FIG. 10. The z component of spin of respective quantum dots as function of T for values of t and t' indicated in Fig. 9 with corresponding symbols. The other parameters are the same as in Fig. 9. See Sec. VI C for details.

the spin-polarized phase (CK′, FK′, or UK′), unless the system is tuned into the spinless $\mathcal{S} = 0$ phase, cf. Fig. 2 and Fig. 5.

Remarkably, in the CK and CK′ phases $\mathcal{S}_{z1} \leqslant 0$, i.e., it has a tendency to align antiparallelly to the leads' majority spins. The QD1 spin polarization is strong in the CK′ phase, while it almost vanishes for the CK one. On the contrary, in the FK/FK′ regime the exchange coupling to the leads changes sign, hence $\mathcal{S}_{z1} \geqslant 0$. Again, in the FK′ phase the absolute value of $\mathcal{S}_{z1}$ is reasonably large and does not vanish even for very small values of frustrating coupling t', while in the FK state it is exponentially suppressed by nonzero temperature.

Similarly to the other regimes, in the UK′ phase $|\mathcal{S}_{z1}| \gg 0$, while in the UK phase $\mathcal{S}_{z1}$ almost vanishes. However, somewhat counterintuitively, $\mathcal{S}_{z1} \geqslant 0$ in the UK/UK′ phase also (that is, the sign is opposite to the one in the CK phase), even though at elevated $T > T^*$ the CK screening takes place there. This is a consequence of the fact that the sign of the exchange field is related to detuning from the PHS. In the model considered in the present paper, the PHS is broken only by t'. Therefore, the formation of the exchange field (also at

QD1) is governed by the molecular trimer states and the sign of t'. As noted in Sec. IV C, for $t' > 0$, in the ground state, $\Delta\varepsilon_{\rm ex}^{\rm GS} > 0$, therefore, the *total* trimer spin z component, $\mathcal{S}_z$, is always negative. What changes between the phases is that in the CK/CK′ phase the trimer spin consists almost exclusively of QD1 spin, $\mathcal{S}_z \approx \mathcal{S}_{z1}$, while in the FK/FK′ and UK/UK′ phases QD2 and QD3 form triplet instead of singlet states and $\mathcal{S}_z \approx \mathcal{S}_{z2} + \mathcal{S}_{z3} - \mathcal{S}_{z1}$. Consequently, the sign of the QD1 spin z component flips at the transition. Notice that should the t' sign happen to change, the exchange field and all the polarizations would change the sign as well (as long as the trimer is at local PHS point).

Furthermore, the side-coupled QDs, QD2 and QD3, are actually even stronger polarized, see Fig. 9 and compare Fig. 10(a) with Fig. 10(b). In fact, in the UK phase and for $T < \Delta\varepsilon_{\rm ex}^{\rm GS}$ they are completely polarized with $\mathcal{S}_{z2} = \mathcal{S}_{z3} = -1/2$ ($\mathcal{S}_{z2} = \mathcal{S}_{z3}$ is a consequence of symmetry and further we only discuss $\mathcal{S}_{z2}$). The value in the FK phase is, on the other hand, $\mathcal{S}_{z2} \approx -1/3$ and decreases slowly with increasing t to obtain $\mathcal{S}_{z2} = 1/4$ for $t \gg U$, which is still significantly larger than for QD1 and causes significant net trimer polarization, $\mathcal{S}_z \approx -1/2$. This kind of magnetic ordering is quite surprising in the Kondo regime, especially at the local PHS point and for very weak values of frustrating coupling t'. Moreover, it is also intriguing whether the realization of a similar state may be possible in correlated, frustrated lattices.

D. Trimer entropy

As a confirmation of the interpretations derived in the preceding sections, in the following we present the results concerning the trimer entropy $\mathbb{S}^{\rm imp}$, defined in Eq. (5). The simple intuition is that $\mathbb{S}^{\rm imp}/k_B$ is a logarithm of the ground-state degeneracy at $T = 0$, and it is increased by the number of trimer states available by thermal fluctuations at elevated temperatures. In Fig. 11(a), we present the results for $p = 0$, which extend the range of validity of earlier results by Mitchell *et al.* [38,39]. In the CK phase, where the ground state is the CK singlet, $\mathbb{S}^{\rm imp}$ practically equals 0. More precisely, it has a small value $\mathbb{S}^{\rm imp} \approx 0.01 k_B$ due to finite temperature used for calculations, $T = 10^{-9}U$. It is even more strongly suppressed in the $\mathcal{S} = 0$ regime, where no small energy scale (such as T_K) is relevant. Then, on the other side of QPT, where the ground state is the spin doublet, the trimer entropy $\mathbb{S}^{\rm imp}/k_B = \ln(2)$, as should be expected. Moreover, exactly at the transition, the degeneracy between the singlet and triplet states gives rise to $\mathbb{S}^{\rm imp}/k_B = \ln(3)$ (at nonzero temperatures this remains true within a small vicinity of the transition).

Due to finite temperature, this result is also valid in the UK phase for $t < t^*$, when the spin triplet formed within the QD2-QD3 subsystem is not yet screened; compare the position of the crossover between the values of $k_B \ln(2)$ and $k_B \ln(3)$ marked with the vertical arrow corresponding to $t = t^*$ in Fig. 11(a). Obviously, at the transition point between this phase and the CK phase, one finds $\mathbb{S}^{\rm imp}/k_B = \ln(4)$. However, since in the FK phase the ground-state degeneracy equals that of the UK phase for $t > t^*$, the FK/UK crossover (its position is indicated in the figure with a dashed line) does not give rise to any signature in the value of $\mathbb{S}^{\rm imp}$, as opposed to the spin expectation value; cf. Fig. 7(a).

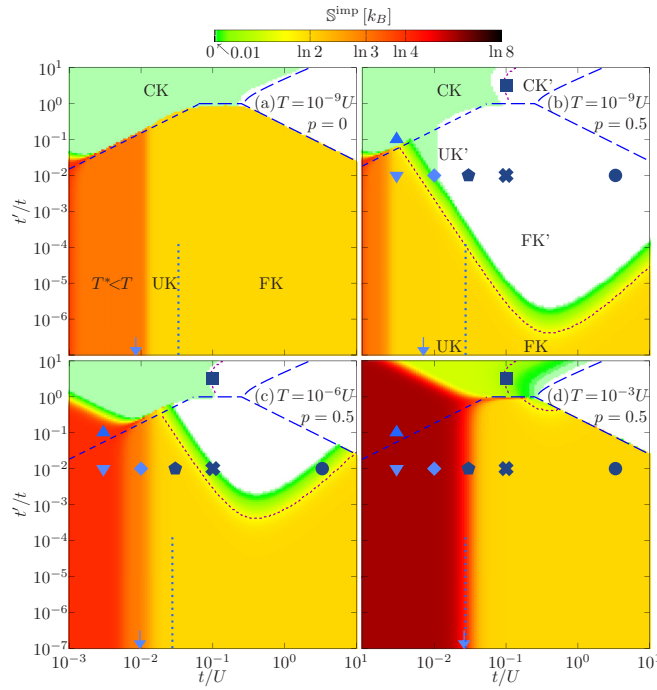

FIG. 11. The entropy of the trimer $\mathbb{S}^{\rm imp}$ as a function of t and t'. Note that the white regions correspond to $\mathbb{S}^{\rm imp} \ll 0.01 k_B$. The parameters are the same as in Fig. 6. The points marked with symbols indicate the values of t and t' for which Fig. 8 is prepared. Small vertical arrows (dotted lines) indicate t^* (t_x) positions, correspondingly.

The landscape changes significantly when the lead magnetization is taken into account. Then, the effective exchange field induced in the trimer, $\Delta\varepsilon_{\rm ex}$, splits the spin multiplets, lifting degeneracy of the ground state. Therefore, whenever $\Delta\varepsilon_{\rm ex} > k_B T$, the trimer entropy drops to zero, manifesting the crossover from a magnetic to nonmagnetic state. This is clearly visible in the FK and FK' phases in Fig. 11(b), as well as for the UK and UK' phases therein. Similarly, while in the nonmagnetic CK phase $\mathbb{S}^{\rm imp} \approx 0.01 k_B$, in the case of magnetic leads and the corresponding CK' regime, the Kondo effect is suppressed when $\Delta\varepsilon_{\rm ex} > T$ and so is the trimer's entropy; cf. Fig. 11(b). Nevertheless, this makes the value of $\mathbb{S}^{\rm imp}$ the same in all magnetic phases and the QPT is visible only as a peak of height $k_B \ln(2)$ in the region of QPT-related degeneracy.

All the above results remain generally correct for higher temperatures, see Figs. 11(c)–11(d), however, phase borders are slightly shifted and regions corresponding to degeneracy at QPT are broadened. Moreover, for sufficiently small values of t and t', the excited states become available, which results in an increase of the trimer's entropy.

E. Other quantities

We found the set of quantities analyzed in previous sections, namely, the linear conductance G, the trimer spin, and its z-component expectation values, $\mathcal{S}$ and $\mathcal{S}_z$, and the trimer entropy $\mathbb{S}^{\rm imp}$ sufficient for complete determination of all the relevant phases. However, in general, the analysis of other physical quantities may also be helpful to pinpoint all the regimes in complex systems. In particular, some of

the magnetic regimes of the system studied here may be recognized in the maps of tunneling magnetoresistance or current spin polarization. However, the characteristic features are restricted to a few of many regimes of the phase diagram and lack some general explanations allowing us to hope that similar features may be relevant for different structures. On the other hand, thermoelectric quantities, such as the Seebeck coefficient, can help determine the phases in strongly particle-hole asymmetric systems, where they tend to have large values and alternating signs in different regimes [108]. The dynamical spin-spin susceptibilities occur to be especially useful for analysis of spin-symmetric non-Fermi-liquid phases [109]. The exceptional usefulness of the quantities chosen here, in particular $\mathcal{S}$ and $\mathcal{S}_z$, stems from the fact that they characterize equally well nonmagnetic as well as fully or partially magnetized structures, which is crucial for determination of the local magnetic texture. This feature may prove important for theoretical characterization of the bulk materials possessing the same correlations as the system described here, in particular frustrated heavy-fermion materials.

VII. CONCLUSIONS

We have determined and analyzed the properties of strongly correlated frustrated QD trimer coupled to ferromagnetic leads. The considerations have been performed by using the NRG method, which was used to calculate the conductance, spin expectation values and the entropy of the analyzed nanostructure. This allowed us to construct the full phase diagram of the system as a function of hoppings between the dots and the temperature, together with the corresponding phase boundaries. We showed that as the hoppings are tuned, at $T = 0$ and for nonmagnetic leads, the system can reveal different phases: the CK phase, the UK phase, the FK phase as well as the non-Kondo spinless phase. These phases are present at finite temperatures, but are not stable in the limit of vanishing temperature in the presence of arbitrarily weak frustrating coupling. We then determined the fate of different Kondo phases in the case of ferromagnetic leads, when the spin splitting of states occurs due to an exchange field. Interestingly, such an exchange field can be generated even at the local PHS point of each dot if the frustrating hopping, which breaks the global PHS, is finite. We showed that the spin polarization of the trimer in the Kondo regime may persist up to sizable temperatures even when the frustrating coupling is very small. This allowed us to extend our conclusions to molecular trimers effectively coupled to one conduction channel, where the frustration is introduced by next-nearest-neighbor hopping. Potentially, these results may be also of relevance for frustrated correlated lattices, where the Kondo screening may coexist with magnetic ordering if some of the local moments are coupled to the electronic bath only indirectly.

ACKNOWLEDGMENTS

This work was supported by the National Science Centre in Poland through Projects No. 2015/19/N/ST3/01030 (K.W.) and No. 2017/27/B/ST3/00621 (I.W.) and by the Deutsche Forschungsgemeinschaft (DFG) through the Cluster of Excellence ML4Q (Grant No. 390534769) (J.K.). K.W. also acknowledges the fellowship of the Alexander von Humboldt Foundation.

[1] H. V. Löhneysen, A. Rosch, M. Vojta, and P. Wölfle, Fermi-liquid instabilities at magnetic quantum phase transitions, Rev. Mod. Phys. **79**, 1015 (2007)

[2] S. Kirchner, S. Paschen, Q. Chen, S. Wirth, D. Feng, J. D. Thompson, and Q. Si, Colloquium: Heavy-electron quantum criticality and single-particle spectroscopy, Rev. Mod. Phys. **92**, 011002 (2020).

[3] M. A. Ruderman and C. Kittel, Indirect exchange coupling of nuclear magnetic moments by conduction electrons, Phys. Rev. **96**, 99 (1954).

[4] T. Kasuya, A theory of metallic ferro- and antiferromagnetism on Zener's model, Prog. Theor. Phys. **16**, 45 (1956).

[5] K. Yosida, Magnetic properties of Cu-Mn alloys, Phys. Rev. **106**, 893 (1957).

[6] S. Friedemann, T. Westerkamp, M. Brando, N. Oeschler, S. Wirth, P. Gegenwart, C. Krellner, C. Geibel, and F. Steglich, Detaching the antiferromagnetic quantum critical point from the Fermi-surface reconstruction in $YbRh_2Si_2$, Nat. Phys. **5**, 465 (2009).

[7] J. Custers, P. Gegenwart, C. Geibel, F. Steglich, P. Coleman, and S. Paschen, Evidence for a Non-Fermi-Liquid Phase in Ge-Substituted $YbRh_2Si_2$, Phys. Rev. Lett. **104**, 186402 (2010).

[8] R. Küchler, C. Stingl, Y. Tokiwa, M. S. Kim, T. Takabatake, and P. Gegenwart, Uniaxial stress tuning of geometrical frustration in a Kondo lattice, Phys. Rev. B **96**, 241110(R) (2017).

[9] Q. Si, Global magnetic phase diagram and local quantum criticality in heavy fermion metals, Physica B **378-380**, 23 (2006).

[10] M. Vojta, From itinerant to local-moment antiferromagnetism in Kondo lattices: Adiabatic continuity versus quantum phase transitions, Phys. Rev. B **78**, 125109 (2008).

[11] P. Coleman and A. H. Nevidomskyy, Frustration and the Kondo effect in heavy fermion materials, J. Low Temp. Phys. **161**, 182 (2010).

[12] Q. Si, J. H. Pixley, E. Nica, S. J. Yamamoto, P. Goswami, R. Yu, and S. Kirchner, Kondo destruction and quantum criticality in Kondo lattice systems, J. Phys. Soc. Jpn. **83**, 061005 (2014).

[13] S. Lucas, K. Grube, C.-L. Huang, A. Sakai, S. Wunderlich, E. L. Green, J. Wosnitza, V. Fritsch, P. Gegenwart, O. Stockert, and H. V. Löhneysen, Entropy Evolution in the Magnetic Phases of Partially Frustrated CePdAl, Phys. Rev. Lett. **118**, 107204 (2017).

[14] B. Sriram Shastry and B. Sutherland, Exact ground state of a quantum mechanical antiferromagnet, Physica B **108**, 1069 (1981).

[15] C. H. Chung, J. B. Marston, and S. Sachdev, Quantum phases of the Shastry-Sutherland antiferromagnet: Application to $SrCu_2(BO_3)_2$, Phys. Rev. B **64**, 134407 (2001).

[16] S. Burdin, D. R. Grempel, and A. Georges, Heavy-fermion and spin-liquid behavior in a Kondo lattice with magnetic frustration, Phys. Rev. B **66**, 045111 (2002).

[17] Y. Motome, K. Nakamikawa, Y. Yamaji, and M. Udagawa, Partial Kondo Screening in Frustrated Kondo Lattice Systems, Phys. Rev. Lett. **105**, 036403 (2010).

[18] T. Sato, F. F. Assaad, and T. Grover, Quantum Monte Carlo Simulation of frustrated Kondo Lattice Models, Phys. Rev. Lett. **120**, 107201 (2018).

[19] A. Benlagra, L. Fritz, and M. Vojta, Kondo lattices with inequivalent local moments: Competitive versus cooperative Kondo screening, Phys. Rev. B **84**, 075126 (2011).

[20] P. P. Deen, A. M. Strydom, S. Paschen, D. T. Adroja, W. Kockelmann, and S. Rols, Quantum fluctuations and the magnetic ground state of $Ce_3Pd_{20}Si_6$, Phys. Rev. B **81**, 064427 (2010).

[21] H. Winkler, S. Laumann, J. Custers, A. Prokofiev, and S. Paschen, Lu and La substituted $Ce_3Pd_{20}Si_6$, Phys. Status Solidi B **247**, 516 (2010).

[22] H. Winkler, K.-A. Lorenzer, S. Laumann, J. Custers, A. Prokofiev, and S. Paschen, Chemical pressure, dilution and disorder in the heavy fermion compounds $Ce_{3-x}La_xPd_{20}Si_6$ ($x = 1/3, 2/3$), J. Phys.: Condens. Matter **23**, 094208 (2011).

[23] A. Tursina, S. Nesterenko, Y. Seropegin, A. M. Strydom, and J. L. Snyman, Crystal structure and physical properties of $CePd_4Sn$: A new magnetically ordered Kondo lattice, J. Alloys Compd. **577**, 677 (2013).

[24] J. Custers, M. Diviši, and M. Kratochvílová, Quantum critical behavior and superconductivity in new multi-site cerium heavy fermion compound Ce_3PtIn_{11}, J. Phys. Conf. Ser. **683**, 012005 (2016).

[25] A. Berton, J. Chaussy, B. Cornut, J. L. Lasjaunias, J. Odin, and J. Peyrard, Specific heat of Ce_3Al_{11} and $CeAl_3$ compounds, J. Magn. Magn. Mater. **15-18**, 379 (1980).

[26] A. K. Mitchell and R. Bulla, Validity of the local self-energy approximation: Application to coupled quantum impurities, Phys. Rev. B **92**, 155101 (2015).

[27] R. Bulla, M. T. Glossop, D. E. Logan, and T. Pruschke, The soft-gap Anderson model: Comparison of renormalization group and local moment approaches, J. Phys.: Condens. Matter **12**, 4899 (2000).

[28] T. Esat, B. Lechtenberg, T. Deilmann, C. Wagner, P. Krüger, R. Temirov, M. Rohlfing, F. B. Anders, and F. S. Tautz, A chemically driven quantum phase transition in a two-molecule Kondo system, Nat. Phys. **12**, 867 (2016).

[29] K. G. Wilson, The renormalization group: Critical phenomena and the Kondo problem, Rev. Mod. Phys. **47**, 773 (1975).

[30] A. Georges, G. Kotliar, W. Krauth, and M. J. Rozenberg, Dynamical mean-field theory of strongly correlated fermion systems and the limit of infinite dimensions, Rev. Mod. Phys. **68**, 13 (1996).

[31] E. Pavarini, D. Vollhardt, E. Koch, and A. Lichtenstein, *DMFT: From Infinite Dimensions to Real Materials* (Verlag des Forschungszentrum Jülich, Jülich, 2018).

[32] R. Žitko and J. Bonča, Numerical renormalization group study of two-channel three-impurity triangular clusters, Phys. Rev. B **77**, 245112 (2008).

[33] E. Vernek, C. A. Büsser, G. B. Martins, E. V. Anda, N. Sandler, and S. E. Ulloa, Kondo regime in triangular arrangements of quantum dots: Molecular orbitals, interference, and contact effects, Phys. Rev. B **80**, 035119 (2009).

[34] T. Numata, Y. Nisikawa, A. Oguri, and A. C. Hewson, Kondo effects in a triangular triple quantum dot: Numerical renormalization group study in the whole region of the electron filling, Phys. Rev. B **80**, 155330 (2009).

[35] A. Oguri, S. Amaha, Y. Nishikawa, T. Numata, M. Shimamoto, A. C. Hewson, and S. Tarucha, Kondo effects in a triangular triple quantum dot with lower symmetries, Phys. Rev. B **83**, 205304 (2011).

[36] M. Koga, M. Matsumoto, and H. Kusunose, Emergent electric polarization by Kondo effect in a triangular triple quantum dot, J. Phys. Soc. Jpn. **81**, 123703 (2012).

[37] C.-Yu. Hsieh, Y.-P. Shim, M. Korkusinski, and P. Hawrylak, Physics of lateral triple quantum-dot molecules with controlled electron numbers, Rep. Prog. Phys. **75**, 114501 (2012).

[38] A. K. Mitchell, T. F. Jarrold, and D. E. Logan, Quantum phase transition in quantum dot trimers, Phys. Rev. B **79**, 085124 (2009).

[39] A. K. Mitchell, T. F. Jarrold, M. R. Galpin, and D. E. Logan, Local moment formation and Kondo screening in impurity trimers, J. Phys. Chem. B **117**, 12777 (2013).

[40] R. López, T. Rejec, J. Martinek, and R. Žitko, SU(3) Kondo effect in spinless triple quantum dots, Phys. Rev. B **87**, 035135 (2013).

[41] S. B. Tooski, B. R. Bułka, R. Žitko, and A. Ramšak, Entanglement switching via the Kondo effect in triple quantum dots, Eur. Phys. J. B **87**, 145 (2014).

[42] G. Yoo, J. Park, S.-S. B. Lee, and H.-S. Sim, Anisotropic Charge Kondo Effect in a Triple Quantum Dot, Phys. Rev. Lett. **113**, 236601 (2014).

[43] S. B. Tooski, A. Ramšak, and B. R. Bułka, Regular and singular Fermi liquid in triple quantum dots: Coherent transport studies, Physica E **75**, 345 (2016).

[44] M. Koga, M. Matsumoto, and H. Kusunose, SU(2)–SU(4) Kondo crossover and emergent electricpolarization in a triangular triple quantum dot, J. Phys. Soc. Jpn. **85**, 063702 (2016).

[45] M. Niklas, A. Trottmann, A. Donarini, and M. Grifoni, Fano stability diagram of a symmetric triple quantum dot, Phys. Rev. B **95**, 115133 (2017).

[46] L.-L. Sun, F. Chi, Z.-G. Fu, S.-C. Yu, L.-M. Liu, and H.-W. Chen, Spin Seebeck effect in a multiple quantum dot molecule with spin-dependent interdot coupling, J. Low Temp. Phys. **194**, 235 (2018).

[47] C.-I. Kim, C.-J. Kang, M.-I. Choe, C.-S. Yun, and J.-K. Ahn, Low-energy doublet states, quantum phase transition, and partial Kondo screening in the triple dot system, Solid State Commun. **289**, 12 (2019).

[48] A. K. Mitchell and D. E. Logan, Two-channel Kondo phases and frustration-induced transitions in triple quantum dots, Phys. Rev. B **81**, 075126 (2010).

[49] R. Žitko and J. Bonča, Fermi-Liquid Versus Non-Fermi-Liquid Behavior in Triple Quantum Dots, Phys. Rev. Lett. **98**, 047203 (2007).

[50] K. Ingersent, A. W. W. Ludwig, and I. Affleck, Kondo Screening in a Magnetically Frustrated Nanostructure: Exact Results on a Stable Non-Fermi-Liquid Phase, Phys. Rev. Lett. **95**, 257204 (2005).

[51] J. Fernández, P. Roura-Bas, A. Camjayi, and A. A. Aligia, Two-stage three-channel Kondo physics for an FePc molecule on the Au(111) surface, J. Phys.: Condens. Matter **30**, 374003 (2018).

[52] E. J. König, P. Coleman, and Y. Komijani, Frustrated Kondo impurity triad: A toy model of deconfinement, arXiv:2002.12338.

[53] J. Kondo, Resistance minimum in dilute magnetic alloys, Prog. Theor. Phys. **32**, 37 (1964).

[54] A. C. Hewson, *The Kondo Problem to Heavy Fermions* (Cambridge University Press, Cambridge, 1997).

[55] P. W. Anderson, A poor man's derivation of scaling laws for the Kondo problem, J. Phys. C: Solid State Phys. **3**, 2436 (1970).

[56] W. Koller, A. C. Hewson, and D. Meyer, Singular dynamics of underscreened magnetic impurity models, Phys. Rev. B **72**, 045117 (2005).

[57] Ph. Nozières and A. Blandin, Kondo effect in real metals, J. Phys. **41**, 193 (1980).

[58] D. S. Saraga and D. Loss, Spin-Entangled Currents Created by a Triple Quantum Dot, Phys. Rev. Lett. **90**, 166803 (2003).

[59] T. Kostyrko and B. R. Bułka, Symmetry-controlled negative differential resistance effect in a triangular molecule, Phys. Rev. B **79**, 075310 (2009).

[60] M. Busl, R. Sánchez, and G. Platero, Control of spin blockade by ac magnetic fields in triple quantum dots, Phys. Rev. B **81**, 121306(R) (2010).

[61] I. Weymann, B. R. Bułka, and J. Barnaś, Dark states in transport through triple quantum dots: The role of cotunneling, Phys. Rev. B **83**, 195302 (2011).

[62] B. R. Bułka, T. Kostyrko, and J. Łuczak, Linear and nonlinear Stark effect in a triangular molecule, Phys. Rev. B **83**, 035301 (2011).

[63] C.-Yu. Hsieh, A. Rene, and P. Hawrylak, Herzberg circuit and Berry's phase in chirality-based coded qubit in a triangular triple quantum dot, Phys. Rev. B **86**, 115312 (2012).

[64] J. M. Taylor, V. Srinivasa, and J. Medford, Electrically Protected Resonant Exchange Qubits in Triple Quantum Dots, Phys. Rev. Lett. **111**, 050502 (2013).

[65] M. Seo, H. K. Choi, S.-Y. Lee, N. Kim, Y. Chung, H.-S. Sim, V. Umansky, and D. Mahalu, Charge Frustration in a Triangular Triple Quantum Dot, Phys. Rev. Lett. **110**, 046803 (2013).

[66] J. Łuczak and B. R. Bułka, Readout and dynamics of a qubit built on three quantum dots, Phys. Rev. B **90**, 165427 (2014).

[67] T. Kuzmenko, K. Kikoin, and Y. Avishai, Magnetically Tunable Kondo–Aharonov-Bohm Effect in a Triangular Quantum Dot, Phys. Rev. Lett. **96**, 046601 (2006).

[68] M. Korkusinski, I. P. Gimenez, P. Hawrylak, L. Gaudreau, S. A. Studenikin, and A. S. Sachrajda, Topological Hunds rules and the electronic properties of a triple lateral quantum dot molecule, Phys. Rev. B **75**, 115301 (2007).

[69] C. Emary, Dark states in the magnetotransport through triple quantum dots, Phys. Rev. B **76**, 245319 (2007).

[70] K. Wrześniewski and I. Weymann, Spin effects in transport through triangular quantum dot molecule in different geometrical configurations, Phys. Rev. B **92**, 045407 (2015).

[71] K. Wrześniewski and I. Weymann, Dark states in spin-polarized transport through triple quantum dot molecules, Phys. Rev. B **97**, 075425 (2018).

[72] K. Wrześniewski and I. Weymann, Current cross-correlations and waiting time distributions in Andreev transport through Cooper pair splitters based on a triple quantum dot system, Phys. Rev. B **101**, 155409 (2020).

[73] M. Vojta, R. Bulla, and W. Hofstetter, Quantum phase transitions in models of coupled magnetic impurities, Phys. Rev. B **65**, 140405(R) (2002).

[74] M. Vojta, Impurity quantum phase transitions, Philos. Mag. **86**, 1807 (2006).

[75] R. Žitko and J. Bonča, Quantum phase transitions in systems of parallel quantum dots, Phys. Rev. B **76**, 241305(R) (2007).

[76] H. Johannesson, N. Andrei, and C. J. Bolech, Critical theory of the two-channel Anderson impurity model, Phys. Rev. B **68**, 075112 (2003).

[77] M. R. Galpin, D. E. Logan, and H. R. Krishnamurthy, Quantum Phase Transition in Capacitively Coupled Double Quantum Dots, Phys. Rev. Lett. **94**, 186406 (2005).

[78] P. P. Baruselli, R. Requist, M. Fabrizio, and E. Tosatti, Ferromagnetic Kondo Effect in a Triple Quantum Dot System, Phys. Rev. Lett. **111**, 047201 (2013).

[79] H. R. Krishna-murthy, J. W. Wilkins, and K. G. Wilson, Renormalization-group approach to the Anderson model of dilute magnetic alloys. II. Static properties for the asymmetric case, Phys. Rev. B **21**, 1044 (1980).

[80] R. Žitko and J. Bonča, Multiple-impurity Anderson model for quantum dots coupled in parallel, Phys. Rev. B **74**, 045312 (2006).

[81] R. Žitko, J. Bonča, A. Ramšak, and T. Rejec, Kondo effect in triple quantum dots, Phys. Rev. B **73**, 153307 (2006).

[82] T. Chowdhury, A. Rosch, and R. Bulla, Competition between Kondo and Kitaev Physics in Kitaev clusters coupled to a fermionic bath, Phys. Rev. B **101**, 115133 (2020).

[83] J. Martinek, M. Sindel, L. Borda, J. Barnaś, R. Bulla, J. König, G. Schön, S. Maekawa, and J. von Delft, Gate-controlled spin splitting in quantum dots with ferromagnetic leads in the Kondo regime, Phys. Rev. B **72**, 121302(R) (2005).

[84] Krzysztof P. Wójcik and I. Weymann, Perfect spin polarization in T-shaped double quantum dots due to the spin-dependent Fano effect, Phys. Rev. B **90**, 115308 (2014).

[85] K. P. Wójcik and I. Weymann, Two-stage Kondo effect in T-shaped double quantum dots with ferromagnetic leads, Phys. Rev. B **91**, 134422 (2015).

[86] I. Weymann and L. Borda, Underscreened Kondo effect in quantum dots coupled to ferromagnetic leads, Phys. Rev. B **81**, 115445 (2010).

[87] F. R. Waugh, M. J. Berry, D. J. Mar, R. M. Westervelt, K. L. Campman, and A. C. Gossard, Single-Electron Charging in Double and Triple Quantum Dots with Tunable Coupling, Phys. Rev. Lett. **75**, 705 (1995).

[88] A. Vidan, R. M. Westervelt, M. Stopa, M. Hanson, and A. C. Gossard, Triple quantum dot charging rectifier, Appl. Phys. Lett. **85**, 3602 (2004).

[89] L. Gaudreau, S. A. Studenikin, A. S. Sachrajda, P. Zawadzki, A. Kam, J. Lapointe, M. Korkusinski, and P. Hawrylak,

Stability Diagram of a Few-Electron Triple Dot, Phys. Rev. Lett. **97**, 036807 (2006).

[90] M. C. Rogge and R. J. Haug, Two-path transport measurements on a triple quantum dot, Phys. Rev. B **77**, 193306 (2008).

[91] L. Gaudreau, A. S. Sachrajda, S. Studenikin, A. Kam, F. Delgado, Y. P. Shim, M. Korkusinski, and P. Hawrylak, Coherent transport through a ring of three quantum dots, Phys. Rev. B **80**, 075415 (2009).

[92] G. Granger, L. Gaudreau, A. Kam, M. Pioro-Ladrière, S. A. Studenikin, Z. R. Wasilewski, P. Zawadzki, and A. S. Sachrajda, Three-dimensional transport diagram of a triple quantum dot, Phys. Rev. B **82**, 075304 (2010).

[93] E. A. Laird, J. M. Taylor, D. P. DiVincenzo, C. M. Marcus, M. P. Hanson, and A. C. Gossard, Coherent spin manipulation in an exchange-only qubit, Phys. Rev. B **82**, 075403 (2010).

[94] L. Gaudreau, G. Granger, A. Kam, G. C. Aers, S. A. Studenikin, P. Zawadzki, M. Pioro-Ladrière, Z. R. Wasilewski, and A. S. Sachrajda, Coherent control of three-spin states in a triple quantum dot, Nat. Phys. **8**, 54 (2011).

[95] F. R. Braakman, P. Barthelemy, C. Reichl, W. Wegscheider, and L. M. K. Vandersypen, Long-distance coherent coupling in a quantum dot array, Nat. Nanotechnol. **8**, 432 (2013).

[96] L. I. Glazman and M. E. Raikh, Resonant Kondo transparency of a barrier with quasilocal impurity states, Pisma Zh. Exp. Teor. Fiz. **47**, 378 (1988) [J. Exp. Theor. Phys. Lett. **47**, 452 (1988)]

[97] F. B. Anders and A. Schiller, Real-Time Dynamics in Quantum-Impurity Systems: A Time-Dependent Numerical Renormalization-Group Approach, Phys. Rev. Lett. **95**, 196801 (2005).

[98] F. B. Anders and A. Schiller, Spin precession and real-time dynamics in the Kondo model: Time-dependent numerical renormalization-group study, Phys. Rev. B **74**, 245113 (2006).

[99] A. Weichselbaum and J. von Delft, Sum-Rule Conserving Spectral Functions from the Numerical Renormalization Group, Phys. Rev. Lett. **99**, 076402 (2007).

[100] O. Legeza, C. P. Moca, A. I. Toth, I. Weymann, and G. Zarand, Manual for the flexible DM-NRG code, arXiv:0809.3143; The code is available at http://www.phy.bme.hu/~dmnrg/.

[101] R. Žitko and T. Pruschke, Energy resolution and discretization artifacts in the numerical renormalization group, Phys. Rev. B **79**, 085106 (2009).

[102] Y. Meir and N. S. Wingreen, Landauer Formula for the Current through an Interacting Electron Region, Phys. Rev. Lett. **68**, 2512 (1992).

[103] A. I. Tóth, C. P. Moca, Ö. Legeza, and G. Zaránd, Density matrix numerical renormalization group for non-Abelian symmetries, Phys. Rev. B **78**, 245109 (2008).

[104] F. D. M. Haldane, Scaling Theory of the Asymmetric Anderson Model, Phys. Rev. Lett. **40**, 416 (1978).

[105] J. Martinek, Y. Utsumi, H. Imamura, J. Barnaś, S. Maekawa, J. König, and G. Schön, Kondo Effect in Quantum Dots Coupled to Ferromagnetic Leads, Phys. Rev. Lett. **91**, 127203 (2003).

[106] P. S. Cornaglia and D. R. Grempel, Strongly correlated regimes in a double quantum dot device, Phys. Rev. B **71**, 075305 (2005).

[107] K. P. Wójcik, Ferromagnets-induced splitting of molecular states of T-shaped double quantum dots, Eur. Phys. J. B **88**, 110 (2015).

[108] T. A. Costi and V. Zlatić, Thermoelectric transport through strongly correlated quantum dots, Phys. Rev. B **81**, 235127 (2010).

[109] Y. Wang, E. Walter, S.-S. B. Lee, K. M. Stadler, J. von Delft, A. Weichselbaum, and G. Kotliar, Global Phase Diagram of a Spin-Orbital Kondo Impurity Model and the Suppression of Fermi-Liquid Scale, Phys. Rev. Lett. **124**, 136406 (2020).